Identification of archeological sites in the Peruvian Amazon using satellite remote sensing

2 authors:

Yaroslav Vasyunin
Paititi Research
10 PUBLICATIONS   **2** CITATIONS

SEE PROFILE

Ceslav Cieslar
3 PUBLICATIONS   **1** CITATION

SEE PROFILE

IDENTIFICATION OF ARCHEOLOGICAL SITES IN THE PERUVIAN AMAZON USING SATELLITE REMOTE SENSING

Ceslav Cieslar[1] and Yaroslav Vasyunin[2]

The Amazon basin is still poorly studied, and new archaeological discoveries will continue to arise. The authors selected the Andean zone of the Manu National Park in Peru as a prominent research area. A substantial archive of geospatial data is collected by integrating it into a multi-user GIS. It includes a digital terrain model, high-resolution aerospace imagery of optical and microwave ranges, and derivative datasets. This paper introduces an original method to outline areas fit for Andean people based on the geospatial analysis in a big data platform. Thus, a settlement suitability map covering over 3000 km² is created and assessed. Furthermore, for areas with high suitability scores, visual interpretation of imagery reveals patterns and features that could indicate archaeological sites. In total, the GIS analysis reveals six sites that could contain human-modified terrain features. The authors also attempt to relate these sites to recorded testimonies from witnesses who encountered large ruins in the mountain rain forest.

1. INTRODUCTION

The archaeology of the Amazon is still poorly known. In particular, there is a scarce theoretical development in the archaeological studies in the Peruvian Amazon. The little relevance granted to this geographical area would be, firstly, due to the low visibility of the archaeological sites, and, secondly, due to complicated conditions of life, transfer, stay, and work [1].

The latest studies show the possibility that the average Amazonian indigenous person at the end of the fifteenth century did not live in an isolated, autonomous village, but instead was part of a regional polity or, at least, articulated with one in broad social networks extended across the region [2]. In 1998 and 1999, two expeditions were that proved the possibility of the river-based goods exchange between Incas and the cultures living in the lower basin of the Amazon. Ancient people might have sailed boats made of totora, a special kind of reed from Lake Titicaca [3]. It is also possible that ancient people inhabited the Amazonian upland far from the main riverine routes. This hypothesis is based on the

[1] Independent Scholar, Switzerland. Email: jellyczez@hotmail.com
[2] Independent Scholar, Italy. Email: yaroslav.vasyunin@gmail.com

discovery of hundreds of geoglyphs with an associated system of roads in the state of Acre, Brazil [4].

A heavily forested, mountainous, and almost uninhabited territory in the Manu National Park in Peru, between Cusco and Madre de Dios regions (Figure 1), could have potentially acted as a barrier and corridor for human societies through time, considering its relevant vicinity to the core of the Inca state. Moreover, two historic Jesuits' manuscripts (*Relazione d'un Miracolo* and *Exsul Immeritus*) [5], [6] and several recent testimonies [7]–[10] point to the high-altitude *selva*, rain forest of southeast Peru, as to the place where a settlement (or settlements) of some developed culture may exist.

To study inaccessible area covering approximately 1500 km^2, it is essential to apply remote sensing technology, widely used across many disciplines, including archaeology.

Remote sensing generally refers to instrument-based techniques measuring properties of objects at a distance, rather than in situ, by utilizing electromagnetic radiation, force fields, or acoustic energy [11]. In this paper, we adhere to the term *Earth remote sensing* (ERS) and limit its meaning to observing the Earth's surface, utilizing only electromagnetic signals recorded on airborne and space-borne platforms. A platform at the lowest flight altitude, such as an aircraft or UAV, achieves the highest spatial resolution but provides only local information, limited by cruising time and radius [12]. Modern ERS satellites enable global measurements with relatively high resolution and are suitable to overcome funding issues while mapping large areas[1].

Figure 1. Location of the research area (red mark). The dot pattern represents the Inca Empire at its greatest extent ca. 1525.

The history of successful applications of ERS for archaeology goes back more than a century, and it proved to be an effective method for archaeological investigations, especially in hardly accessible regions like tropical forests [13]. The principle behind archaeological ERS, as explained in [14], is the following: ancient human transformations of the landscape left subtle features called *marks* that are only visible when viewed from above. For example, caused by subsurface archaeological remains, these marks can be observed as differences in plant growth or variations [15] of micro-topographic relief visible by shadowing [16]. They can be revealed as *anomalies* in a signal of different spectral ranges, recorded by an ERS sensor, which finally allows detection of linked human-made features, buried and exposed.

ERS, applied in archaeology, can be divided into four distinct groups: photography, multi/hyperspectral imaging, synthetic aperture radar (SAR), and light detection and ranging (lidar) [13].

---

[1] https://droneapps.co/price-wars-the-cost-of-drones-planes-and-satellites/

Historically, photography was the first ERS method, implemented by passive film-based cameras sensitive mainly to the visible part of the electromagnetic spectrum [17]. Historic film photographs taken by airborne platforms and declassified spy satellites decades ago are still used by archaeologists who study changes in land cover that have occurred over the past century [18].

Multi and hyperspectral imaging involves the passive acquisition of electromagnetic energy in different ranges simultaneously, from visible to far-infrared, which has a higher potential to detect archaeological sites and monuments than photography [19]. It is especially true for hyperspectral sensors with more than hundreds of spectral bands, which were successfully used to indicate the presence of underground buried structures, mainly by detection of crop marks in farmland [20]. Hyperspectral surveys are usually conducted by airborne platforms because hyperspectral space-borne instruments are limited due to technical constraints. Moreover, practical issues of hyperspectral sensor costs, data volumes, and data processing mechanisms need to be addressed for operational use and favor multispectral systems [21]. Multispectral sensors, especially space-borne, having fewer spectral bands, became the most popular imaging technique in archaeology. They are applied to detect and identify archaeological features, paleo-landscape analysis and reconstruction, looting monitoring and assessment, urbanization mapping, risk monitoring and assessment, and cultural heritage management and conservation [13].

Another emerging imaging technique is realized with SAR — an active type of ERS. In its simplest form, SAR is a radar whose output product is a two-dimensional mapping of "radar brightness" that resembles a black-and-white aerial photograph [22]. SAR can sense a target under all-weather conditions at any time of day or night and even penetrate soil and vegetation, depending on the wave frequency and target properties [23]. A significant amount of studies demonstrated that SAR is superior at detecting buried features, soil marks, and relief for archaeological purposes [24], [25], with notable implications for archaeology in tropical forests, where SAR data was used to detect ancient settlements in densely vegetated areas [26]–[28]. However, applications of SAR in mountainous areas are limited due to inherent radiometric and geometric distortions in reconstructed images [29], [30].

Imaging lidar — the optical analog of SAR — transmits visible or near-infrared pulses to the ground and takes backscattered echoes of radiation to reconstruct 3d topography [31]. The ability of lidar to penetrate overlying vegetation and forest canopies generated a fundamental shift in Mesoamerican archaeology and transformed research in forested areas worldwide [32]–[34]. However, lidar imaging is mainly airborne due to the practical limitations of satellite platforms, which imposes restrictions on its application in inaccessible distant regions or low-budget projects.

From the user point of view, access to ERS data and delivery systems, in particular to space-borne data sets, became transparent and straightforward [35]. Nowadays, governmental organizations, such as NASA[1], Natural Resources Canada[2], and the European Space Agency[3] freely and openly distribute low-to-moderate-resolution ERS imagery covering

---

[1] https://earthdata.nasa.gov
[2] https://www.eodms-sgdot.nrcan-rncan.gc.ca/index_en.jsp
[3] https://earth.esa.int/eogateway

the whole globe. To acquire high-resolution data, users refer to the commercial ERS market [36], rich in data suppliers, such as Maxar[1], Planet[2] , and Airbus Defense & Space[3].

The combination of ERS data from multiple sensors and platforms, together with other geospatial data and ground observations, should provide more precise insight and contextual information about Earth's surface anomalies [37], [38]. It can be done in a *Geographic Information System* (GIS), which is a "computer-based system to aid in the collection, maintenance, storage, analysis, output, and distribution of spatial data and information." [39] The early pioneers of archaeological GIS quickly recognized that it was more than a data management tool. The analytic power of GIS to advance understandings of past landscapes was demonstrated in several works, collected in [40]. Now GIS, ERS, and other digital technologies became standard and well-routinized tools in archaeology [41], [42].

The use of GIS by archaeologists is typically grouped into three broad categories: inventory, spatial analysis, and mapmaking [43]. Archaeological features can be extracted from imagery using GIS-aided manual interpretation or automatic detection following image enhancement. The spatial analysis used for prospecting of new archaeological sites has a long and successful track record [43]–[46]. The advent of open-source software, including GIS, triggered a vast research volume in different fields and disciplines [47]. Combined with ERS data, which became an accessible and profitable commodity [48], it dramatically facilitates archaeological explorations.

Petabytes of openly available *big data* from space-borne Earth observation missions led to data processing and analysis issues. A robust and expandable cloud platform, Earth Engine was designed by Google to tackle these issues — it empowers a broad audience that lacks the technical capacity needed to utilize traditional supercomputers or large-scale cloud computing resources [49]. Thus, the platform was successfully applied to the detection of buried Neolithic tells and the investigation of the urban sprawl impact in the vicinity of archaeological sites and monuments [50]. However, literature research in Scopus[4] performed in June 2020 retrieves just three papers related to "Earth Engine" and "archaeology" keywords, which makes it a prospective study direction.

In this work, we perform low-cost research based on non-invasive technology of Earth remote sensing (ERS), an open-source geographic information system (GIS), and a big data platform Google Earth Engine (GEE), to locate potential human-modified sites in a forested mountainous region of Peru. We develop a cloud GIS infrastructure for multi-user work on the project and integrate ERS imagery with various geospatial data sets, such as digital elevation models (DEM) and historical maps. A novel predictive technique that allows detecting areas suitable for ancient settlements is put into action based on GEE scripts, open to the public. The most prominent areas are manually studied using the available imagery and maps, which reveal marks that could indicate archaeological sites.

---

[1] https://www.maxar.com

[2] https://www.planet.com

[3] https://www.airbus.com/space.html

[4] Abstract and citation database of peer-reviewed journals: https://www.scopus.com/

2. MATERIALS AND METHODS

2.1. GIS Infrastructure

As the research team was scattered worldwide, this study's first step was creating a GIS that enables simultaneous work on geospatial layers. Such implementations have already been realized in [51], [52]. Our spatial infrastructure's core became the Relational Database Service (RDS) platform from Amazon[1], allowing cost-effective and straightforward configuration, use, and scaling of relational databases in the cloud. The platform is equipped with an open-source RDBMS PostgreSQL[2] with the PostGIS[3] extension to work with spatial data. The overall architecture of the implemented GIS is provided in Figure 2.
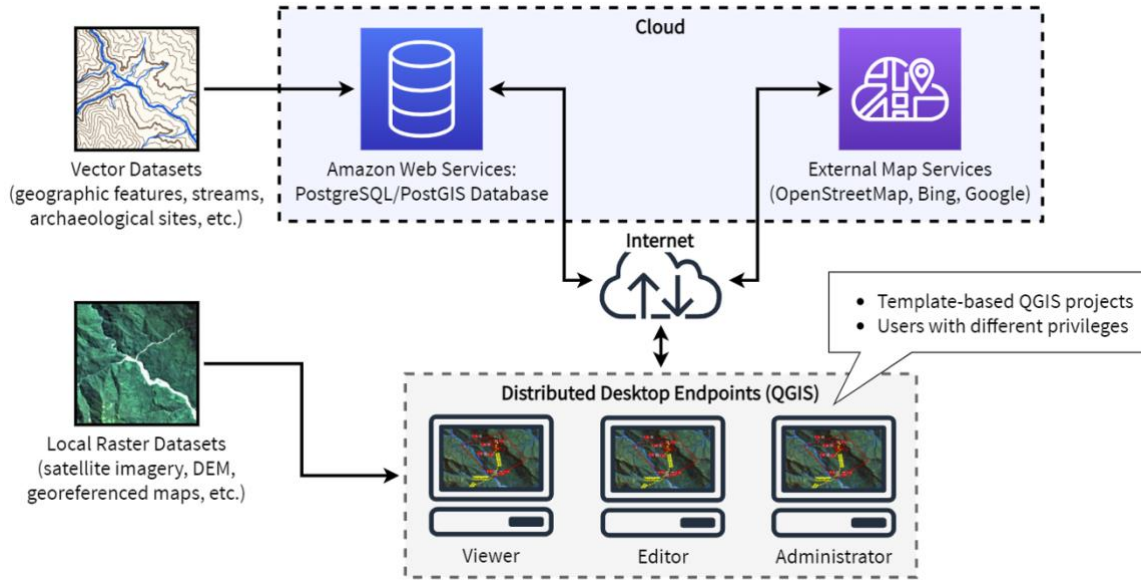

Figure 2. The architecture of the implemented multi-user GIS database for desktop systems, which is based on open-source technologies.

The front end for interacting with geospatial information in the database is the desktop open-source, cross-platform software QGIS[4]. To ensure security, connecting to the database is limited to specific IP addresses and configured user roles, listed by ascending privileges: Reader, Editor, and Administrator. All geospatial data used in the study are divided into vector and raster categories. Vector layers are updated frequently and stored centrally in RDS without duplication on local computers. However, a set of raster data is updated and processed rarely, mainly at the beginning of the project. As a compromise, to reduce the number of information transmitted via the Internet, it was decided to copy the same set of raster data on each local machine. Thus, when a user launches QGIS and enters a password, they see a map consisting of both local raster layers and remote vector layers.

---

[1] https://aws.amazon.com/rds/

[2] https://www.postgresql.org

[3] https://postgis.net

[4] https://qgis.org/

It is worth mentioning that GIS is not an end in itself. It serves for the optimal representation of the finished geospatial information embedded in it by developers and researchers, who analyze and interpret this information based on their experience, intuition, and assumptions.

2.2. Data Collection and Overview Study

The research area extended over ca. 8,000 km², lies where the southeastern Peruvian Andes transitions to the rainforests of the Amazon basin, on the border between Cusco and Madre de Dios regions. Western mountainous side, *sierra*, varies in altitudes from 2,000 m to 4,000 m, covered chiefly by low grass and shrubs. Eastern mountain selva goes down to 1000 m and has a very high density of woody vegetation — more than 75%[1].

As in any project on the analysis of poorly studied, almost uncharted territories, work begins with collecting all available territorial data, which are then ingested in GIS. Thereupon, it becomes clear what methods of geospatial analysis apply to the data collected. All the data sets collected by authors fit into two groups by their map detail level. The *overview level* has moderate spatial resolution and covers the whole research region, while the *detailed level* with high spatial resolution clarifies only specific spots.

It is worth noting the difficulty of obtaining cloud-free satellite images in the visible and near-infrared bands for the territory of interest. In this regard, the authors developed an algorithm for the Earth Engine platform that allows generating high-quality image mosaics (Landsat-8 and Sentinel-2 image collections). The publicly available algorithm allows every researcher to quickly download not only cloud-free satellite mosaics but a set of primary geospatial data, such as land cover types and DEM, to any world region [54].

The subsequent processing of the acquired DEM with the QGIS geo-processing toolkit allowed us to create derivative data sets: hydrographic network and morphometric terrain parameters (slope and aspect).[2] A list of the collected and created (derived) datasets is given in Table 1.

---

[1] Percentage of horizontal ground in each 30-m pixel covered by woody vegetation greater than 5 meters in height [53]

[2] https://docs.qgis.org/3.16/en/docs/training_manual/processing/index.html

Table 1. Primary datasets used in the research.

RASTER DATASETS: REMOTE SENSING IMAGERY

Platform name	Platform type[1]	Spectral range[2]	GSD, m²	Cloud-free coverage, km	Temporal range	Reference	Note
Landsat-8	SB	V-NIR-SWIR	15,0	8,000	2013-2019	landsat.gsfc.nasa.gov	cloudless mosaic created in GEE
WorldView-2	SB	V	1,0	7,000	2010-2014	www.bing.com/maps	high-resolution imagery base map from Microsoft
UAVSAR	AB	MW	10,0-20,0	7,000	2014	uavsar.jpl.nasa.gov	polarimetric L-band images in three polarization RGB color overlay: HH, HV, VV
PlanetScope	SB	V-NIR	3,0	5,800	2018-2019	www.planet.com	
RapidEye	SB	V-NIR	5,0	4,700	2012	www.planet.com	
GeoEye-1	SB	V	0,5	95	2016-2017	www.maxar.com	

RASTER DATASETS: OTHER TYPES

Product name	Type	GSD, m	Coverage	Reference	Note
Copernicus Global Land Service: Land Cover 100m: collection 3: epoch 2019: Globe	land cover	100,0	8,000	[55]	
NASA SRTM3 SRTMGL1	terrain	30,0	8,000	[56]	
Landsat Vegetation Continuous Fields (VCF)	land cover	30,0	8,000	[53]	
Slope	terrain	30,0	8,000		derived from DEM in QGIS
Aspect	terrain	30,0	8,000		derived from DEM in QGIS
Annual insolation	terrain	30,0	8,000		the direct incoming solar radiation, derived from DEM with the Area Solar Radiation tool in ArcGIS Pro

VECTOR DATASETS

Product name	Vector data type	Note
Contour lines	linear	50 m vertical distance, derived from DEM in QGIS
Stream network	linear	derived from DEM with the Hydrology toolset of ArcGIS Pro - a set of vector features representing the linear hydrological network
Inca roads	linear	result of a joint interpretation of high-resolution satellite imagery and terrain datasets; contains mostly hypothetical trails

---

[1] SB – space-borne; AB – air-borne
[2] V – visible; (N/SW)IR – near/short-wave infrared; MW – microwave

2.3. Predicting Modelling

Mountain environments tend to constrain movements [57]. As a critical physiographic feature of South America, the Andes acted as a barrier and corridor for human societies and their displacements, enabling the interactions between *costa* (the Pacific coast), sierra, and selva [58]–[60]. In mountainous areas, some authors used a combined GIS and remote sensing approach to predict ancient human frequentations [61], [62]. We decided to extrapolate their approach for our research area, identified in the Introduction.

We performed a preliminary study of well-known Inca ruins, such as Machu Picchu and Vilcabamba (see the complete list in the Appendix A). Their coordinates were collected by overpass turbo, a web-based data filtering tool for OpenStreetMap[1] with the following query:

```
[out:json][timeout:25];
(node["historic:civilization"~"inca",i];
 way["historic:civilization"~"inca",i];
 relation["historic:civilization"~"inca",i];);
out body; >; out skel qt;
```

As seen from Figure 3, they show relation to terrain morphology, namely slope that fits the range approx. 0-20˚. To assure the derived conclusions, we assumed that the settling patterns of small modern local communities did not change significantly. We retrieved 15738 samples of small Andean settlements from OpenStreetMap[2]. For each point, we created a 50-meter-radius buffer and calculated terrain morphology values [54], which result is represented in Figure 4.
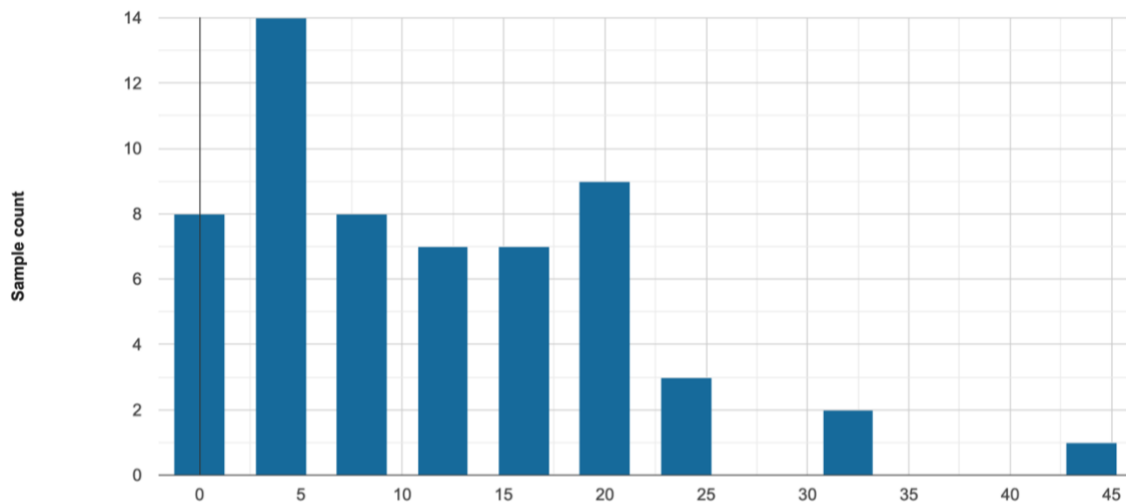

Figure 3. Median slope angle for Inca archaeological sites, 59 samples.

---

[1] https://overpass-turbo.eu/
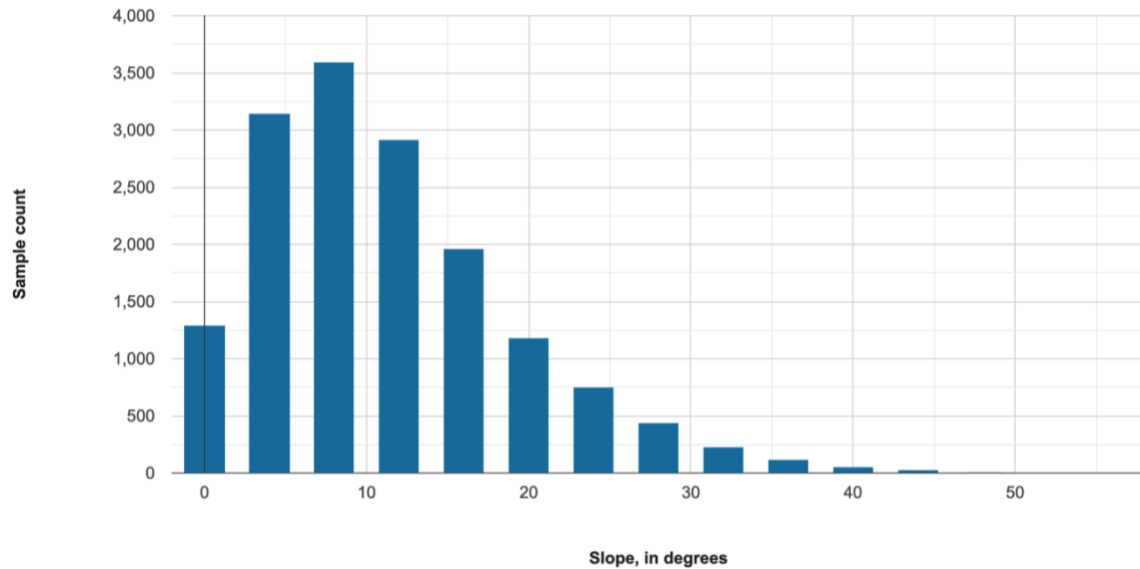[2] https://www.openstreetmap.org/

Figure 4. Median slope angle for small modern Andean settlements, 15738 samples.

Compared to other terrain-related factors taken into accounts, such as incoming solar radiation and aspect, slope gives the most evident relationship with the distribution of inhabited places. It is also easy to compute slope maps in an open-source QGIS instead of computationally intensive solar radiation tools, e.g., available in commercial software ArcGIS[1].

Based on the obtained relationship between slope and populated places in the Andes, the authors created a *Slope Steepness/Settlement Suitability Map* (SSM — Appendix B), which divides the entire study area into five distinct categories by slope steepness: gentle (0-10˚), slightly steep (10-20˚), steep (20-30˚), highly steep (30-60˚), and precipitous (60-90˚). The relation between slope categories and suitability is the following:

- Gentle slope → Highly suitable
- Slightly steep → Suitable
- Steep → Poorly suitable
- Highly steep and Precipitous → Unsuitable

Thus, the efforts to collect and analyze high-resolution ERS data were focused only on the territories mapped as *highly suitable* and *suitable*. It reduced the search area from 8000 km² down to 2350 sq. km.

2.4. High-resolution Data Interpretation

Existing analytical tools for object detection associated with digital remote sensing data, such as road or building detection, usually fail when targeting elusive archaeological traces. [38]. Moreover, the possibility of locating new archaeological sites from aerial or satellite

---

[1]   https://desktop.arcgis.com/en/arcmap/latest/tools/spatial-analyst-toolbox/an-overview-of-the-solar-radiation-tools.htm

imagery is highly dependent on various parameters, such as image spatial resolution, the extension of buried sites, ground characteristics, illumination conditions, and view geometry [14].

A thorough visual interpretation of all available spatial data, specifically of high-resolution, became the basis of our research approach. The criteria to identify potential unknown archaeological sites were the position in the basin of the Nistron river, on terrain of *highly suitable* and *suitable classes*, a water source presence, and the dominant position over the surroundings. Undoubtedly, this is a subjective way, but it is the human eye that can notice subtle marks in images, linking them with the surrounding context (Figure 5).
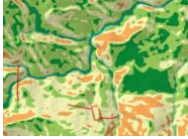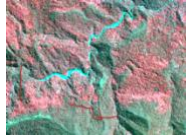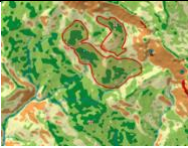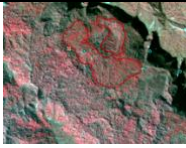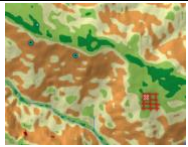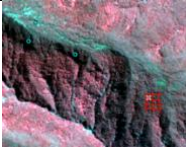
Figure 5. One of the identified features — a subtle dark grid (3 hectares) formed by the play of shadows in the forest 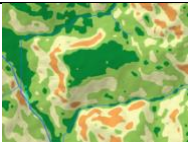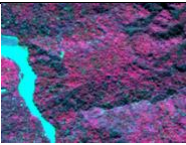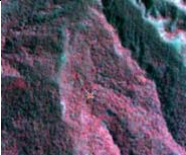canopy, which could correspond to an underlying human-made structures that affect the distribution and growth of trees. Image from WorldView-2 satellite, acquired 2010-10-28. © 2017 DigitalGlobe, © 2017 HERE

In GIS, the entire study area was divided into 1x1 km squares. We analyzed an area of about 3000 km^2, with a particular focus on the areas highlighted by the SSM — for which we have acquired high-resolution commercial data. Different team members connected to the database with their local GIS were marking "suspicious" image patterns as new vector features, saving them in the database. Since the target's appearance was unknown, we tried to discern any visual marks present in the images in the visible, near-infrared, and microwave ranges. The bird's eye perspective and switching between different datasets helped to get a holistic understanding of the observed territory. Upon completion of the analysis of each square, it was marked as "studied." Of course, it was necessary to repeatedly re-check the studied squares: each image interpreter has a different, unique experience, and various factors, including simple fatigue, influence their performance. Therefore, mutual control became is an essential part of the work.

3. RESULTS

Six areas of interest (AOI) in the basin of the Nistron river were identified as potential candidates. Subtle image features were revealed inside these areas, which may refer to buried or semi-buried human-made structures. Table 2 describes every AOI.

Table 2. Identified areas of interest.

N.	SSM view	Pseudo-color view	Approx. area, ha	Description[1]
1			300	1050–1250 m MSL; linear and point features visible in MS imagery.
2			80	1460–1800 m MSL; linear features in SAR and MS optical imagery.
3			300	1360–1660 m MSL; abundance of linear and point features visible in MS imagery.
4			100	2700–3170 m MSL: linear features visible in SAR and MS imagery.
5			50	900–950 m MSL; absence of features in imagery, but the position is advantageous over surroundings.
6			50	1150–1350 m MSL; linear features visible in SAR imagery and a point feature visible in MS imagery.

---

[1] MSL — mean sea level; SAR — synthetic aperture radar; MS — multi-spectral.

4. DISCUSSION

4.1. Limitations of the Proposed Approach

Based on the insights given in [26]–[28], it was initially presumed that microwave L-band images (UAVSAR[1]) would penetrate through vegetation and expose bare terrain patterns. However, this approach did not work in the study region due to physical limitations: L-band waves do not penetrate through the thick foliage. Moreover, the image quality is heavily affected by geometric distortions caused by rugged mountain terrain. The amount of image noise made it hard to discern clear signals from the surface level. Thus, the authors switched to visual and near-infrared image analysis.

The archaeological features, i.e., the ancient human transformations of the landscape, are visible in imagery as subtle differences in vegetation growth or micro-topographic relief variations. The dense forests in the research area significantly obstruct their identification, and natural shapes can be misinterpreted as artificial. The authors expect to have false positives in the recognized linear features.

With the lack of evidence on the existence of archaeological sites, the authors relied heavily on geoinformation modeling. As the SRTM digital terrain model became the basis of this study, it is worth mentioning that 30-m ground resolution does not allow the detailed study of terrain morphometry. Thus, small-size archaeological sites cannot be discovered with SRTM. The authors assumed that the potential sites would be large enough to be expressed in this dataset.

4.2. Testimonies

Until today, the only known large ancient settlement in the basin of the Madre de Dios river are the ruins of Mameria, discovered in the 1970s by Herbert Cartagena [8], [10, pp. 113–116]. However, there are a few unverified testimonies describing the existence of a larger settlement hidden in the selva of the Manu National Park. Such testimonies were reported by Landa [7, pp. 56, 19, 51–53, 57], and Palkiewicz & Kaplanek [9, p. 374]. They narrow down the research area to the Nistron (Maestron) river basin in the western Manu National Park.

The AOI 3 turned to be the most promising site due to its position between all the areas described in the testimonies and the presence of several recognized image features. It has favorable terrain conditions as it has a dominant position with mountains that limit its western part. It should provide natural protection, the abundance of waterfalls and water supply, as mentioned in several testimonies. See the visual presentation of the finding is in the Figure 6 and different representations of the site in the Appendix C

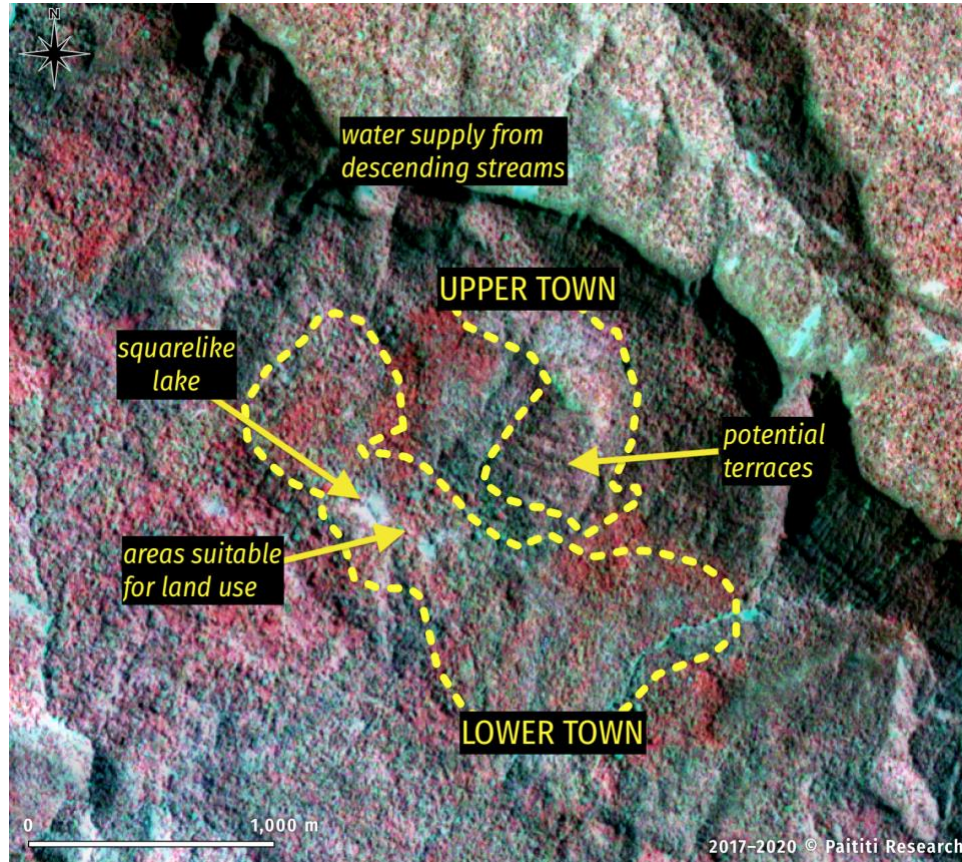---

[1] https://uavsar.jpl.nasa.gov/

Figure 6. A potential location of a large site in the AOI 3 on the left side of the Nistron river. Yellow boundaries highlight suitable flat areas: the "upper town" (about 20 ha, 1650 m above MSL) dominates the surroundings, protected from north-east by a 350-meter-tall abrupt "wall" of a mountain range; the "lower town" (about 100 ha, 1300 m above MSL) has a good water supply from descending streams — we suppose it could have been used for agricultural needs. Underlying multi-spectral image from PlanetScope satellite, acquired Sep 28, 2019, by courtesy of Planet Labs, Inc.

5. CONCLUSIONS

Six areas with potential archaeological sites were identified in the Manu National Park[1] based on the combined analysis of terrain data, remote sensing imagery, and other cartographic information. On some of these sites, subtle image anomalies were recognized, potentially indicating underlying human-made structures.

One of those areas, of approximately 2 km² at 1360–1660 m above mean sea level, is selected as the most prominent because it corresponds to the descriptions from Jesuits' manuscripts (*Relazione d'un Miracolo* and *Exsul Immeritus*), recorded testimonies of a few local natives, and has high suitability score according to the designed geospatial modeling. Moreover, after the visual interpretation of high-resolution multi-spectral satellite images of

---

[1] Manu Province in the Madre de Dios region, Peru

the area, several linear marks that could indicate potential archaeological features are recognized in this area.

In addition, the complete geospatial database of the vast, poorly mapped Peruvian area, created in this work, gives a unique holistic understanding of that environment. It is enabled by a multi-user GIS that connects researchers from different places in the world. On the one hand, the collected data brings value for future studies in the region, such as for the Manu National Park administration to preserve biodiversity. On the other hand, the developed open-source GIS workflow can be applied outside of this research area, and it is not limited to only archaeology.

The authors are aware that the presented evidence is not yet conclusive and that more additional data is required to be collected. The further investigation, either by fieldwork activities or by an aerial lidar survey able to penetrate through thick vegetation, would be crucial in the verification of the results of this work, in the understanding of the settlement patterns on the eastern Andean side, and in the interaction between selva and sierra people.

6. ACKNOWLEDGMENTS

7. REFERENCES

[1] H. Tantaleán, "Un panorama de la teoría arqueológica en el Perú de comienzos del siglo XXI," *Discursos sur*, no. 5, pp. 201–243, Jul. 2020, doi: 10.15381/dds.v0i5.18150.

[2] M. Heckenberger and E. G. Neves, "Amazonian Archaeology," *Annu. Rev. Anthropol.*, vol. 38, no. 1, pp. 251–266, Oct. 2009, doi: 10.1146/annurev-anthro-091908-164310.

[3] J. Blashford-Snell and R. Snailham, *East to the Amazon: In Search of Great Paititi and the Trade Routes of the Ancients*. London: John Murray, 2002.

[4] M. Pärssinen, W. Balée, A. Ranzi, and A. Barbosa, "The geoglyph sites of Acre, Brazil: 10 000-year-old land-use practices and climate change in Amazonia," *Antiquity*, vol. 94, no. 378, pp. 1538–1556, Dec. 2020, doi: 10.15184/aqy.2020.208.

[5] "Relazione d'un miracolo… nel Regno di Paÿtiti a canto del Perù [Report of a miracle… in the Kingdom of Paÿtiti near Peru]," Archivum Romanum Societatis Iesu, Perù, 19, ff. 38-41, 1567/1625.

[6] L. Laurencich-Minelli, "Traduzione in italiano del quaderno Exsul Immeritus Blas Valera Populo Suo [Italian translation of the notebook Exsul Immeritus Blas Valera Populo Suo]," in *Exsul immeritus blas valera populo suo e Historia et rudimenta linguae piruanorum: Indios, gesuiti e spagnoli in due documenti segreti sul Perù del XVII secolo*, CLUEB, 2005, pp. 307–340. doi: 10.1400/104366.

[7] C. N. Landa, *Paititi en la bruma de la historia [Paititi in the mist of history]*. Arequipa: Cuzzi, 1983.

[8] G. Deyermenjian, "Mameria: an Incan Site Complex in the High-Altitude Jungles of Southeast Peru," *Athena Review*, vol. 3, no. 4, pp. 80–88, 2003.

[9] J. Palkiewicz and A. Kaplanek, *El Dorado. Polowanie Na Legende [El Dorado. Hunt For The Legend]*. Poznan: Wydawnictwo Zysk i S-ka, 2005.

[10] J. Edigo, *Paititi - la ciudad perdida [Paititi - the lost city]*. Lulu.com, 2017.

[11] V. V. Salomonson, "Remote sensing, historical perspective," *Encyclopedia of Remote Sensing*. Springer, New York, pp. 684–690, 2014. doi: 10.1007/978-0-387-36699-9_158.

[12] H. P. Röser and M. Von Schönermark, "Comparison of remote sensing experiments from airborne and space platforms," *Acta Astronautica*, vol. 39, no. 9–12, pp. 855–862, 1996, doi: 10.1016/S0094-5765(97)00070-2.

[13] L. Luo *et al.*, "Airborne and spaceborne remote sensing for archaeological and cultural heritage applications: A review of the century (1907–2017)," *Remote Sensing of Environment*, vol. 232, no. March, p. 111280, 2019, doi: 10.1016/j.rse.2019.111280.

[14] R. Lasaponara and N. Masini, "Remote Sensing in Archaeology: From Visual Data Interpretation to Digital Data Manipulation," in *Satellite Remote Sensing: A New Tool for Archaeology*, vol. 16, no. 5, R. Lasaponara and N. Masini, Eds. Dordrecht: Springer, 2012, pp. 3–16. doi: 10.1007/978-90-481-8801-7.

[15] R. Lasaponara and N. Masini, "Detection of archaeological crop marks by using satellite QuickBird multispectral imagery," *Journal of Archaeological Science*, vol. 34, no. 2, pp. 214–221, 2007, doi: 10.1016/j.jas.2006.04.014.

[16] D. Tapete, F. Cigna, and D. N. M. Donoghue, "'Looting marks' in space-borne SAR imagery: Measuring rates of archaeological looting in Apamea (Syria) with TerraSAR-X Staring Spotlight," *Remote Sensing of Environment*, 2016, doi: 10.1016/j.rse.2016.02.055.

[17] J. N. Hampton, "Aerial Reconnaissance for Archaeology: Uses of the Photographic Evidence," *The Photogrammetric Record*, vol. 9, no. 50, pp. 265–272, 1977, doi: 10.1111/j.1477-9730.1977.tb00087.x.

[18] A. Agapiou, D. D. Alexakis, A. Sarris, and D. G. Hadjimitsis, "Colour to Greyscale Pixels: Re-seeing Greyscale Archived Aerial Photographs and Declassified Satellite CORONA Images Based on Image Fusion Techniques," *Archaeological Prospection*, vol. 23, no. 4, pp. 231–241, 2016, doi: 10.1002/arp.1536.

[19] A. Beck, "Archaeological applications of multi / hyper-spectral data – challenges and potential," in *Remote Sensing for Archaeological Heritage Management. Occasional Publication of the Aerial Archaeology Research Group No. 3*, 2011, pp. 87–97.

[20] D. Cerra, A. Agapiou, R. M. Cavalli, and A. Sarris, "An objective assessment of hyperspectral indicators for the detection of buried archaeological relics," *Remote Sensing*, vol. 10, no. 4, pp. 1–25, 2018, doi: 10.3390/rs10040500.

[21] M. Govender, K. Chetty, and H. Bulcock, "A review of hyperspectral remote sensing and its application in vegetation and water resource studies," *Water SA*, vol. 33, no. 2, pp. 145–151, 2007, doi: 10.4314/wsa.v33i2.49049.

[22] K. Raney, "Radar, Synthetic Aperture," *Encyclopedia of Remote Sensing*. Springer, New York, pp. 536–547, 2014. doi: 10.1007/978-0-387-36699-9.

[23] F. Wiig *et al.*, "Mapping a subsurface water channel with X-band and C-band synthetic aperture radar at the iron age archaeological site of 'Uqdat al-Bakrah (Safah), Oman," *Geosciences (Switzerland)*, vol. 8, no. 9, 2018, doi: 10.3390/geosciences8090334.

[24] D. Tapete and F. Cigna, "COSMO-SkyMed SAR for detection and monitoring of archaeological and cultural heritage sites," *Remote Sensing*, vol. 11, no. 11, 2019, doi: 10.3390/rs11111326.

[25] D. Tapete and F. Cigna, "Trends and perspectives of space-borne SAR remote sensing for archaeological landscape and cultural heritage applications," *Journal of Archaeological Science: Reports*, vol. 14, pp. 716–726, 2017, doi: 10.1016/j.jasrep.2016.07.017.

[26] F. Yakam-Simen, E. Nezry, and J. Ewing, "Legendary lost city found in the Honduran tropical forest using ERS-2 and JERS-1 SAR imagery," in *International Geoscience and Remote Sensing Symposium (IGARSS)*, 1999, vol. 5, pp. 2578–2580. doi: 10.1109/igarss.1999.771582.

[27] W. Saturno, T. L. Sever, D. E. Irwin, B. F. Howell, and T. G. Garrison, "Putting Us on the Map: Remote Sensing Investigation of the Ancient Maya Landscape," in *Remote Sensing in Archaeology*, 1st ed., J. Wiseman and F. El-Baz, Eds. New York: Springer, 2007, pp. 137–160. doi: 10.1007/0-387-44455-6_6.

[28] E. Moore, T. Freeman, and S. Hensley, "Spaceborne and Airborne Radar at Angkor: Introducing New Technology to the Ancient Site," in *Remote Sensing in Archaeology*, 1st ed., J. Wiseman and F. El-Baz, Eds. New York: Springer, 2007, pp. 185–216. doi: 10.1007/0-387-44455-6_8.

[29] T. Bayer, R. Winter, and G. Schreier, "Terrain influences in SAR backscatter and attempts to their correction," *IEEE Transactions on Geoscience and Remote Sensing*, vol. 29, no. 3, pp. 451–462, 1991, doi: 10.1109/36.79436.

[30] C. Jung and P. Rebillard, "Effects Of Slopes And Relief Two-dimensional Spatial Frequencies On Spaceborne Sar Imagery," in *International Geoscience and Remote Sensing Symposium, "Remote Sensing: Moving Toward the 21st Century,"* 1988, vol. 3, pp. 1575–1578. doi: 10.1109/IGARSS.1988.569526.

[31] D. M. Tratt, "Emerging Technologies, Lidar," *Encyclopedia of Remote Sensing*. Springer, New York, pp. 177–185, 2014. doi: 10.1007/978-0-387-36699-9.

[32] A. F. Chase, D. Z. Chase, C. T. Fisher, S. J. Leisz, and J. F. Weishampel, "Geospatial revolution and remote sensing LiDAR in mesoamerican archaeology," *Proceedings of the National Academy of Sciences of the United States of America*, vol. 109, no. 32, pp. 12916–12921, 2012, doi: 10.1073/pnas.1205198109.

[33] T. Inomata *et al.*, "Monumental architecture at Aguada Fénix and the rise of Maya civilization," *Nature*, no. November 2019, 2020, doi: 10.1038/s41586-020-2343-4.

[34] A. Rowlands and A. Sarris, "Detection of exposed and subsurface archaeological remains using multi-sensor remote sensing," in *Journal of Archaeological Science*, vol. 34, no. 5, 2007, pp. 795–803. doi: 10.1016/j.jas.2006.06.018.

[35] R. Weaver, "Data Access," *Encyclopedia of Remote Sensing*. Springer, New York, pp. 119–121, 2014. doi: 10.1007/978-0-387-36699-9.

[36] W. Gail, "Commercial Remote Sensing," *Encyclopedia of Remote Sensing*. Springer, New York, pp. 78–83, 2014. doi: 10.1007/978-0-387-36699-9.

[37] D. Tapete, V. Banks, L. Jones, M. Kirkham, and D. Garton, "Contextualising archaeological models with geological, airborne and terrestrial LiDAR data: The Ice Age landscape in Farndon Fields, Nottinghamshire, UK," *Journal of Archaeological Science*, vol. 81, pp. 31–48, 2017, doi: 10.1016/j.jas.2017.03.007.

[38] K. Lambers, "Airborne and Spaceborne Remote Sensing and Digital Image Analysis in Archaeology," in *Digital Geoarchaeology. Natural Science in Archaeology*, C. Siart, M.

Forbriger, and O. Bubenzer, Eds. Cham: Springer, 2018, pp. 109–122. doi: 10.1007/978-3-319-25316-9_7.

[39] P. Boldstad, *GIS Funfamentals, A First Text on Geographic Information Systems*, 5th ed. White Bear Lake: XanEdu, 2016.

[40] K. M. S. Allen, S. W. Green, and E. B. W. Zubrow, Eds., *Interpreting Space: GIS and Archaeology*. London: Taylor & Francis, 1990.

[41] M. C. L. Howey and M. Brouwer Burg, "Assessing the state of archaeological GIS research: Unbinding analyses of past landscapes," *Journal of Archaeological Science*, vol. 84, pp. 1–9, 2017, doi: 10.1016/j.jas.2017.05.002.

[42] A. V. Postnov and E. G. Vergunov, "Подготовка специализированных ГИС для археологии [Preparation of specialized GIS for archeology]," in *Методика археологических исследований Западной Сибири [Methodology of archaeological research in Western Siberia]*, vol. 904, L. V. Tataurova, Ed. Omsk: Favorit, 2005, pp. 57–64.

[43] G. T. Edward, "Recent directions and future developments in geographic information systems for historical archaeology," *Historical Archaeology*, vol. 50, no. 3, pp. 24–49, 2016.

[44] B. Bobowski, "The history of digital methods in archeology (1951-1999) [Past Perfect metod cyfrowych w archeologii (1951-1999)]," *Echa Przeszlosci*, vol. 22, no. 1, pp. 13–52, 2019, doi: 10.31648/ep.4827.

[45] M. D. McCoy and T. N. Ladefoged, "New developments in the use of spatial technology in archaeology," *Journal of Archaeological Research*, vol. 17, no. 3, pp. 263–295, 2009, doi: 10.1007/s10814-009-9030-1.

[46] F. Estrada-Belli and M. Koch, "Remote Sensing and GIS Analysis of a Maya City and Its Landscape: Holmul, Guatemala," in *Remote Sensing in Archaeology*, 1st ed., J. Wiseman and F. El-Baz, Eds. New York: Springer, 2007, pp. 263–281. doi: 10.1007/0-387-44455-6_11.

[47] G. von Krogh and S. Spaeth, "The open source software phenomenon: Characteristics that promote research," *Journal of Strategic Information Systems*, vol. 16, no. 3, pp. 236–253, 2007, doi: 10.1016/j.jsis.2007.06.001.

[48] M. Craglia and K. Pogorzelska, "The Economic Value of Digital Earth," in *Manual of Digital Earth*, H. Guo, M. F. Goodchild, and A. Annoni, Eds. Singapore: Springer, 2020, pp. 623–643. doi: 10.1007/978-981-32-9915-3_19.

[49] N. Gorelick, M. Hancher, M. Dixon, S. Ilyushchenko, D. Thau, and R. Moore, "Google Earth Engine: Planetary-scale geospatial analysis for everyone," *Remote Sensing of Environment*, vol. 202, pp. 18–27, 2017, doi: 10.1016/j.rse.2017.06.031.

[50] A. Agapiou, "Remote sensing heritage in a petabyte-scale: satellite data and heritage Earth Engine© applications," *International Journal of Digital Earth*, vol. 10, no. 1, pp. 85–102, 2017, doi: 10.1080/17538947.2016.1250829.

[51] Z. Magyari-Sáska, "Developing and implementing multiuser, fully relational gis database for desktop systems using open source technologies," *Geographia Technica*, vol. 10, no. 2, pp. 59–65, 2015.

[52] D. (eHealth A. Sonoiki, "An Open Source Approach to Multi-user Distributed Geospatial Data Management," *FOSS4G, Open Source Geospatial Foundation (OSGeo)*, 2016. https://av.tib.eu/media/20348 (accessed Jul. 22, 2020).

[53] J. O. Sexton *et al.*, "Landsat Tree Cover Continuous Fields." University of Maryland, College Park, 2015.

[54] Y. Vasyunin and V. Lobanov, "Paititi Research: Data Processing Scripts for Earth Engine." figshare, 2021. doi: 10.6084/m9.figshare.14421125.v1.

[55] M. Buchhorn *et al.*, "Copernicus Global Land Service: Land Cover 100m: collection 3: epoch 2019: Globe." Zenodo, 2020. doi: 10.5281/zenodo.3939050.

[56] "NASA Shuttle Radar Topography Mission Global 1 arc second." NASA LP DAAC, 2013. doi: 10.5067/measures/srtm/srtmgl1.003.

[57] D. Visentin *et al.*, "Prehistoric landscapes of the Dolomites: Survey data from the highland territory of Cadore (Belluno Dolomites, Northern Italy)," *Quaternary International*, vol. 402, pp. 5–14, 2016, doi: 10.1016/j.quaint.2015.10.080.

[58] V. A. Durán *et al.*, "'To and fro' the southern Andean highlands (Argentina and Chile): Archaeometric insights on geographic vectors of mobility," *Journal of Archaeological Science: Reports*, vol. 18, no. February, pp. 668–678, 2018, doi: 10.1016/j.jasrep.2017.05.047.

[59] C. Stanish *et al.*, "Tiwanaku trade patterns in southern Peru," *Journal of Anthropological Archaeology*, vol. 29, no. 4, pp. 524–532, 2010, doi: 10.1016/j.jaa.2010.09.002.

[60] D. A. Contreras, "How far to conchucos? A GIS approach to assessing the implications of exotic materials at chavín de huántar," *World Archaeology*, vol. 43, no. 3, pp. 380–397, 2011, doi: 10.1080/00438243.2011.605841.

[61] K. Kompatscher and M. Hrozny Kompatscher, "Dove piantare il campo: modelli insediativi e di mobilità nel Mesolitico in ambiente alpino," *Preistoria alpina*, vol. 42, no. 42, pp. 137–162, 2007.

[62] S. Caracausi, G. L. F. Berruti, S. Daffara, D. Bertè, and F. Rubat Borel, "Use of a GIS predictive model for the identification of high altitude prehistoric human frequentations. Results of the Sessera valley project (Piedmont, Italy)," *Quaternary International*, vol. 490, no. November 2017, pp. 10–20, 2018, doi: 10.1016/j.quaint.2018.05.038.

APPENDIX A. LIST OF THE KNOWN ARCHAEOLOGICAL SITES

Coordinates: longitude, latitude (WGS84)	Type	Name
-78.18911009041936211 -9.54916617589478633	Inca	unknown
-65.88649965857210589 -22.51079371023869768	Inca	unknown
-72.11288030339787269 -13.30098187108892382	Inca	unknown
-71.96997944139567949 -13.50830249957862073	Inca	unknown
-73.95403729365048662 -13.65389959829188626	Inca	unknown
-77.07198444695121964 -12.06723787728948238	pre-Inca	unknown
-77.07215274547407091 -12.06227902089199588	pre-Inca	unknown
-74.01429306297312394 -13.60065919632519638	Inca	Acllahuasi
-65.84857780000000105 -22.02524539999999931	Inca	Calahoyo
-78.42842652190149977 0.00018832541572125	Inca	Catequilla
-74.85800133182270599 -12.73478481678160179	Inca	Chunkana
-71.56055627202657377 -16.44512874384819412	pre-Inca	Complejo arqueologico Kakallinca
-71.56353417186322474 -16.44021836937946190	pre-Inca	Complejo arqueologico Kasapatac
-71.56254170001484738 -16.44353695077025890	pre-Inca	Complejo arqueologico Tres Cruces
-77.07269238428330027 -11.98450875741795763	pre-Inca	Huaca Aznapuquio
-77.07107192555619690 -11.88957033583235123	Inca	Huaca Tambo Inga
-76.81635102476359123 -9.87541968860685415	Inca	Huánuco Pampa
-72.06351646239625097 -13.36353541577751258	Inca	Machu Qollqa
-71.60638889999999890 -14.96861110000000039	Inca	María Fortaleza
-71.56500409999999590 -14.92476779999999970	pre-Inca	Mauk'allaqta
-72.19708230495820089 -13.33048485382195203	Inca	Moray
-65.88572323756328331 -22.51232257670934445	Inca	Moreta
-75.17824304409330693 -14.55299338856019098	Inca	Nazca Lines
-72.92796036703208529 -13.11109954629611174	Inca	Ñusta Hispana
-78.99691147679186543 -2.90740317403922788	Inca	Parque Arqueologico Pumapungo
-72.42502207191016339 -13.23102744054985891	Inca	Patallacta
-72.53152510035695855 -13.20632265580255371	Inca	Phuyupatamarka
-72.26088324196463475 -13.25638700781221324	Inca	Pinkuylluna
-71.84319517809181832 -13.40821846561960662	Inca	Pisaq
-70.68378789999999867 -34.06834589999999707	Inca	Pucará del Cerro Grande de La Compañía
-71.96216028138753984 -13.48335108060471832	Inca	Puka Pukara
-75.82896960048169888 -13.70519710552497905	Inca	Pukatampu
-76.93599554467552082 -12.04962003679565008	Inca	Puruchuco
-71.97175117653151233 -13.51034624781295612	Inca	Q'enqo Chico
-71.97049307681248820 -13.50901159324859790	Inca	Q'enqo Grande
-72.26210343998327801 -13.61450273616862638	Inca	Qollmay
-74.86079831300708065 -12.73796948248669381	Inca	Qorimina
-73.96390900000000101 -13.83710969999999918	Inca	Raqa Raqaypata
-71.36929837921640285 -14.17496004399198917	Inca	Raqch'i
-74.06619411790684637 -13.96872877319371398	Inca	Ruinas de Inti Watana
-78.43087192407350017 0.01335577461163674	Inca	Rumicucho
-72.50139498618257505 -13.22845600726906667	Inca	Runkuraqay
-71.99244283544612699 -13.52935116256297654	Inca	S.A. Pokenkancha
-71.99469277501910369 -13.53154425677604600	Inca	S.A. Puquin / Hermanos Ayar
-71.98042427751055072 -13.50732942924198987	Inca	Saksaywaman
-71.25511125581158467 -29.88552875250002216	Inca	Sitio Paleoindio de Asentamiento y Necrópolis El Olivar

−71.96736911450786067	−13.47888675402604974	Inca	Tampu Mach'ay
−75.68501510000000110	−11.47505529999999929	Inca	Tarmatambo
−74.85795984135754111	−12.73757134621275355	Inca	Uchkus Inkañan
−72.93186783394334327	−13.09827929063190410	Inca	Vitcos
−72.49564965592215060	−13.02076404242771446	Inca	Wamanmarka
−73.20710649185696184	−12.90207456860550117	Inca	Willkapampa
−72.42322342843154104	−13.23537539901991522	Inca	Willkarakay
−72.53640625789245178	−13.19293752860655111	Inca	Wiñay Wayna
−71.98914906044983297	−13.53419116329233951	Inca	Z.A. Qhataq'asapatallaqta
−76.77242694332446149	−12.50955480261609587	Inca	Zona Arqueológica Bandurria
−66.08736319999999864	−19.81218150000000122	Inca	Zona Arqueologica Chaquilla
−76.90104949435638559	−12.25696776933438059	pre-Inca	Zona Arqueológica Monumental Pachacámac
−74.06795083729583951	−13.91477942317083993	Inca chancas	Zona Arquologica de Cachipata

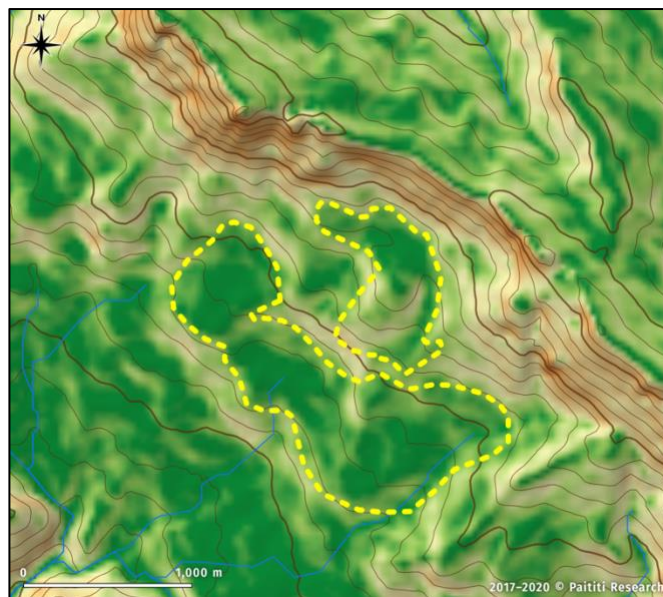# APPENDIX B. SLOPE STEEPNESS/SETTLEMENT SUITABILITY MAP

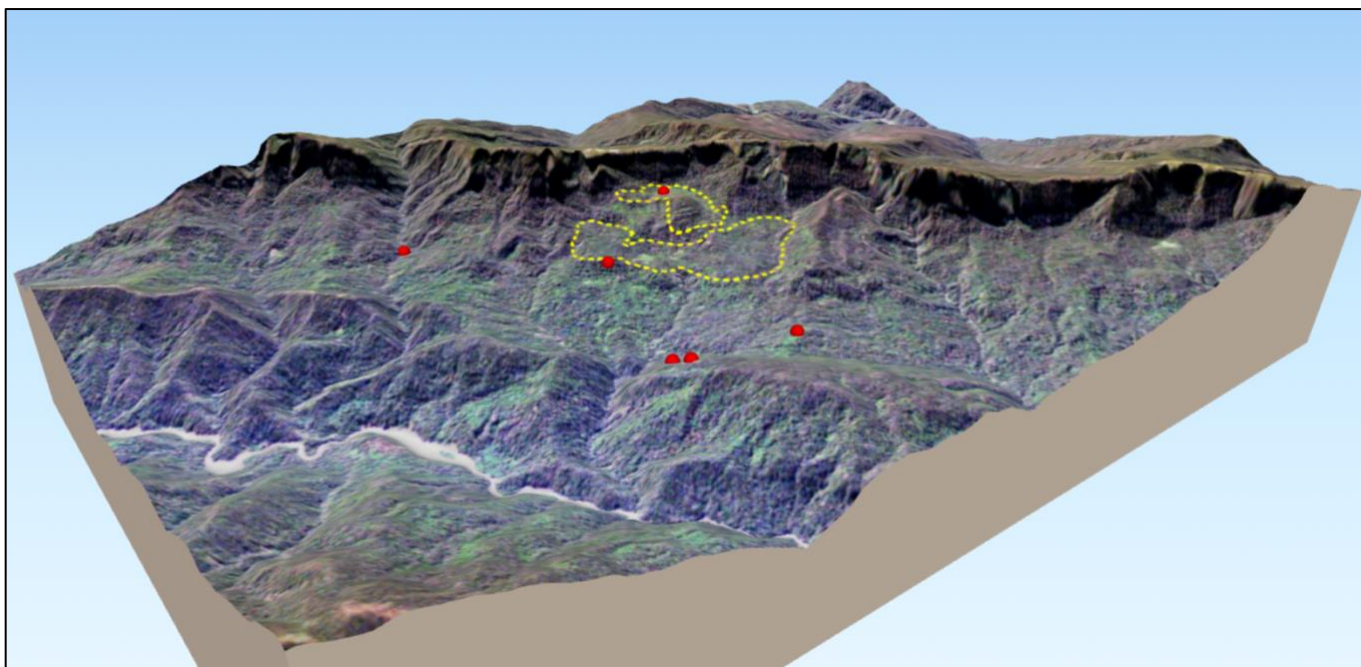**It predicts suitable areas of the search for archaeological sites, which are depicted in green color.**
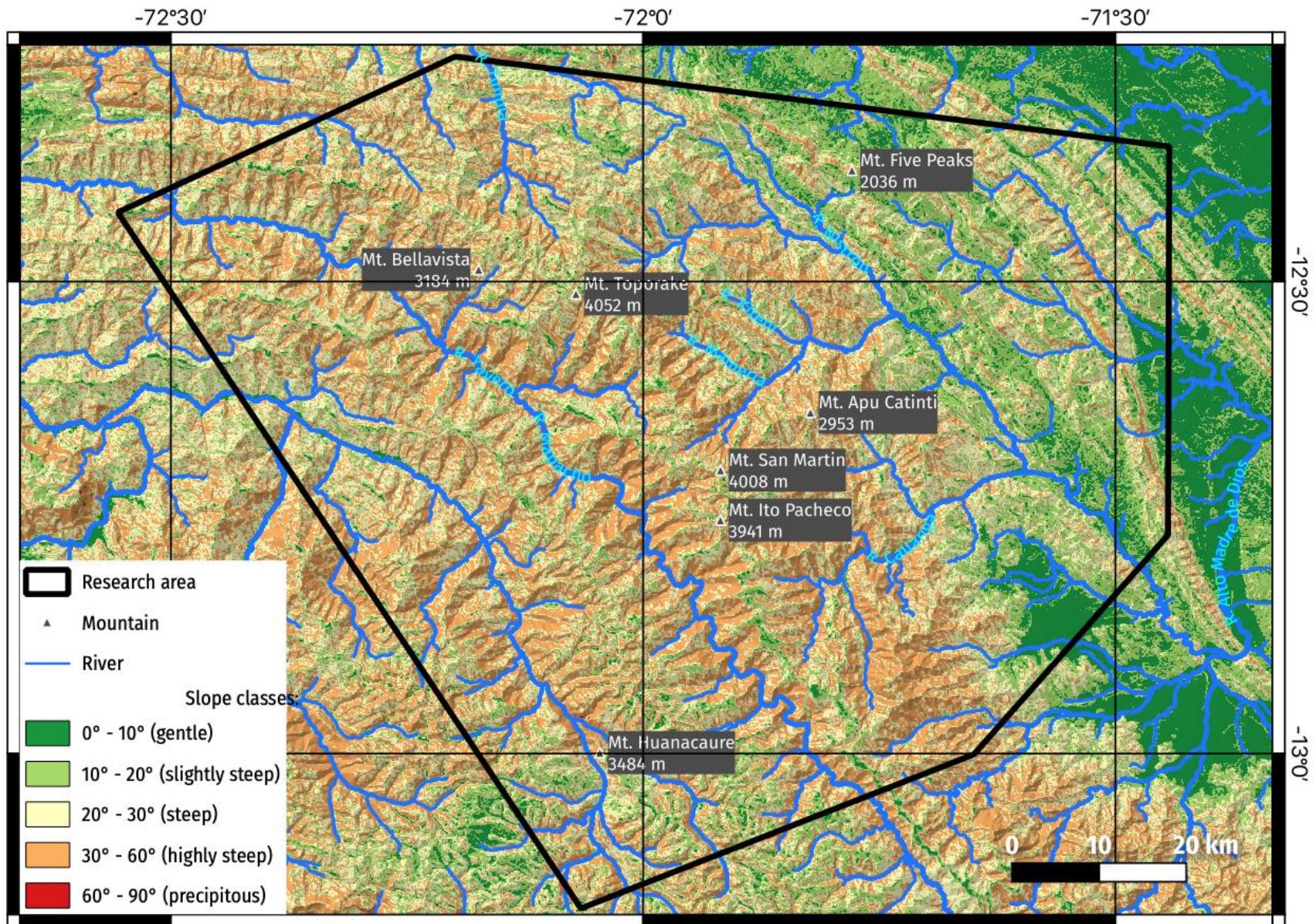
Natural-color image of the AOI 3 from PlanetScope satellite, acquired Sep 28, 2019, by courtesy of Planet Labs, Inc.

Settlement Suitability Map. A potential large site is located in the "green" zone with a high suitability score, mostly defined by a low slope grade.

Overview of the AOI 3 and its surroundings in 3D: NASA SRTM3 SRTMGL1 digital elevation model with superimposed PlanetScope image, acquired Sep 28, 2019, by courtesy of Planet Labs, Inc. Red markers correspond to potential archaeological features identified in the imagery.